JOURNAL OF CATALYSIS **168,** 42–50 (1997)
ARTICLE NO. CA971538

Characterization of Graphite-Supported Palladium–Cobalt Catalysts by Temperature-Programmed Reduction and Magnetic Measurements

F. B. Noronha,* M. Schmal,* C. Nicot,† B. Moraweck,†,[1] and R. Fréty‡

*NUCAT-COPPE/EQ, Universidade Federal do Rio de Janeiro, Ilha do Fundao, COPPE, C.P. 68502, CEP 21941, Rio de Janeiro, Brazil; †Institut de Recherches sur la Catalyse, 2 Avenue Albert Einstein, F 69626 Villeurbanne Cedex, France; and ‡Laboratoire d'Application de la Chimie à l'Environnement, Université Claude Bernard, 43 Boulevard du 11 novembre 1918, F 69622 Villeurbanne Cedex, France

Received March 15, 1996; revised August 5, 1996; accepted November 18, 1996

Graphite-supported cobalt, palladium, and cobalt–palladium systems were prepared by a simple impregnation technique and submitted to hydrogen reduction in a temperature-programmed mode. Using X-ray diffraction to define the structure of the calcined precursors, magnetic measurements to determine the amount of metallic cobalt formed after reduction, and analysis of the gaseous medium during the reduction, a general model for the reduction of the graphite supported catalysts has been suggested. At room temperature, both pure PdO and PdO associated with Co_3O_4 are reduced to the metallic state. In the case of bimetallic systems, a fraction of Co_3O_4 in close proximity or interfaced with PdO can be reduced to the metallic state and to CoO species, demonstrating a strong catalytic effect of palladium on the reduction of cobalt oxides. At temperatures between 298 and 500 K, depending on the catalyst formulation, the presence of metallic palladium promotes the reduction of a large fraction of oxidized cobalt. At higher reduction temperature, at least two competitive phenomena were detected: direct reduction of the residual oxidized cobalt by the graphite, leading to carbon monoxide and dioxide formation, and hydrogasification of the graphite catalyzed by the supported metals, leading mainly to methane formation. Together with a possible short-range palladium-activated hydrogen migration, at low and moderate temperatures, long-range migration of particles is necessary to explain the observations. These migrations, in turn, favor the formation of bimetallic particles, after reduction at 773 K.

INTRODUCTION

Modification of supported cobalt catalysts has been the subject of several investigations. The nature of the support (1–4) and the addition of both alkaline earth metals (5, 6) and noble metals (7–10) were found to change the activity and the selectivity of cobalt catalysts in CO hydrogenation. For example, it was proposed that the addition of a noble metal increases the reducibility of cobalt oxides, leading to a larger fraction of metallic cobalt (8–14). Since the catalytic hydrogenation of carbon monoxide with cobalt catalysts is affected by the extent of reduction (15–17), the presence of a "reduction promoter" could play an important role in the catalytic behavior of the catalyst.

Guczi *et al.* (9) studied the structure and the catalytic activity of alumina supported Pt–Co bimetallic catalysts in the CO/H_2 reaction. On Pt/Al_2O_3 and on Pt-rich catalysts, oxygenates were the main products, whereas hydrocarbon selectivity increased with the cobalt loading. These variations in selectivity were attributed to different oxidation states of cobalt. Indeed, TPR results showed a platinum-assisted reduction of cobalt oxide and suggested the formation of Pt–Co bimetallic particles. On the other hand, Iglesia *et al.* (18) showed that the presence of Ru in supported cobalt catalysts not only enhanced the reduction of the cobalt oxide but also inhibited carbon deposition during Fischer–Tropsch synthesis. They suggested that the C_5^+ selectivity is due to the higher stability of Co–Ru bimetallic catalysts against coking.

Although numerous companies have suggested that catalysts containing both Pd and Co can be useful in important process like gas exhaust cleaning and selective hydrogenations (19–22), no recent claims on such systems in the $CO + H_2$ reaction has been patented. Furthermore, there are only a few studies about Pd–Co bimetallic catalysts in the literature (10, 11, 23–25). However, while Co-based catalyst usually produces long-chain hydrocarbons, methanol can be selectively formed over Pd catalysts in CO hydrogenation (26). The addition of palladium to Co/CeO_2 catalysts resulted in the formation of ethanol (11) on the $CO + H_2$ reaction. In this case too, TPR analysis showed that palladium addition enhanced the reduction of cobalt, in agreement with an intimate contact between both metallic species. While the changes in selectivity due to the addition of a second metal to cobalt are well accepted, the formation of bimetallic particles has not been clearly proven and the mechanism of their formation is not fully understood.

The aim of this work is to describe the state of the calcined precursors and to follow the activation of supported palladium–cobalt catalysts in order to understand

[1] To whom correspondence should be addressed.

0021-9517/97 $25.00

the chemistry involved during their reduction. We chose graphite as a support, because an interaction of cobalt with either Al_2O_3 (27–29) or SiO_2 (30, 31) could lead to the formation of unreducible cobalt species, affecting the nature and the importance of Pd–Co interaction. Thus, an intimate contact between cobalt and palladium on graphite would probably be obtained more easily as a result of both a weaker interaction between each of the metal precursors with the support and a higher mobility of supported species on graphite. TPR associated with mass spectroscopy (MS) and magnetic measurements are used to study the activation of graphite-supported palladium–cobalt catalysts.

EXPERIMENTAL

Catalyst Preparation

A high surface area graphite (Lonza HSAG II; BET surface area, 130 m^2/g) was used as support. The monometallic and the bimetallic catalysts were prepared by the incipient wetness impregnation (or coimpregnation) of the graphite with aqueous solutions of $Pd(NO_3)_2 \cdot 2H_2O$ (Strem Chemicals) and $Co(NO_3)_2 \cdot 6H_2O$ (Merck), followed by drying at 393 K for 16 h and calcination in air at 673 K for 2 h. The catalysts and their metal contents are presented in Table 1.

X-Ray Diffraction (XRD)

X-ray diffraction patterns of the calcined catalyst precursors were obtained using a Philips PW 1710 diffractometer (Cu $K\alpha$ radiation). The X-ray tube was operated at 45 kV and 35 mA, and the X-ray diagram was scanned with a step size of 0.02° (2θ) (1 s per step) from 10 to 80° (2θ).

Electron Microscopy

Calcined and reduced/passivated catalyst samples were suspended in anhydrous ethanol. A drop of the suspension was deposited on a carbon-coated copper grid. Transmission electron microscopy (TEM) measurements were performed using a JEOL 100 CX electron microscope (3 nm resolution). High-resolution transmission electron microscopy (HRTEM) carried out with a JEOL 2010 (0.2 nm resolution) was used in specific cases. EDX-STEM analysis of the catalysts was performed on a VG HB 501 scanning electron microscope fitted with an energy dispersive Tracor X-ray spectrometer. The analysis was performed either in scanning mode to measure the mean composition of large areas of the sample or in spot mode to determine the composition of selected particles.

TABLE 1

Catalyst Composition

Catalyst	Composition (wt%)	
	Pd	Co
Pd/g	2.26	—
$Pd_{33}Co_{67}$/g	3.12	3.44
$Pd_{16}Co_{84}$/g	3.37	9.96
Co/g	—	3.61

Note: Pd_xCo_y : x and y represent the atomic percentage of Pd and Co.

Temperature-Programmed Reduction Followed by TCD (TPR1)

The TPR analysis and the equipment were similar to that described previously (32). Before reduction, the catalysts were dehydrated at 423 K in flowing argon. A mixture of 1% hydrogen in argon (30 ml/min) was passed through the catalyst sample. Before heating the catalyst at 10 K/min from room temperature to 1173 K, the hydrogen consumption at room temperature was carefully recorded. Water vapor formed during the reduction was retained at room temperature in a trap containing zeolite 3A. The catalyst weight was selected to ensure that 0.01 g of metallic active phase was present in all experiments.

TPR Followed by TCD and Mass Spectroscopy (TPR2)

Due to problems associated with graphite gasification (33, 34), the TCD detector was coupled, on line, to a quadrupole mass analyzer (Balzers, QMS 420, linked to a Quadstar V3 Analytical System). The reducing gas and the reduction conditions were similar to the ones described for the TPR linked only to a TCD detector, except that water vapor formed during reduction was not trapped.

Magnetic Measurements

Magnetic measurements were carried out to verify the extent of reduction of the cobalt species (after different temperatures of reduction) and eventually confirmed the formation of a palladium–cobalt alloy. The cell for magnetic measurements was linked, on line, to the TPR equipment, fitted with TCD and MS detectors. Such an arrangement ensured that the reduction could be stopped by quickly cooling the sample in order to measure the magnetic properties of cobalt at well-defined reduction steps.

The magnetization was measured at 298 K, using the extraction method of Weiss (35, 36). Saturation magnetization (M_s) was obtained by plotting the magnetization M against $1/H$ (H, magnetic field) and by extrapolating to $1/H = 0$. M_s allowed us to calculate the amount of metallic cobalt and, by comparison with the total amount of cobalt, the degree of reduction of the catalyst. For this calculation, the value of the magnetic moment associated with one cobalt atom must be known. Since the magnetic moment associated with one cobalt atom was found to increase with dilution of cobalt in palladium from 1.7 μB in pure cobalt to 9–10 μB in the

most diluted alloys, the correction of the magnetic moment proposed by Bozorth *et al.* (37) was used to calculate the reduction degree of cobalt in the bimetallic catalysts.

RESULTS

X-Ray Diffraction

Figure 1 shows the X-ray diffraction patterns for the calcined precusors which match perfectly with that of PdO, Co_3O_4 (JCPDS files 41–1107 and 42–1467, respectively), and graphite, even in the case of the bimetallic precursors.

Electron Microscopy

Images obtained by HRTEM for the calcined $Pd_{16}Co_{84}$/G catalyst displayed reticular planes fringes. The interplanar distances and the directions of the plane traces correspond well with that expected for pure PdO and Co_3O_4. This observation is in full agreement with X-ray diffraction results.

Large area analyses by EDX indicated that both cobalt and palladium-rich areas existed in this sample, although isolated particles with pure cobalt and pure palladium were hardly observed. Furthermore, spot-mode analyzes often suggested that a physical contact between PdO and Co_3O_4 particles exist.

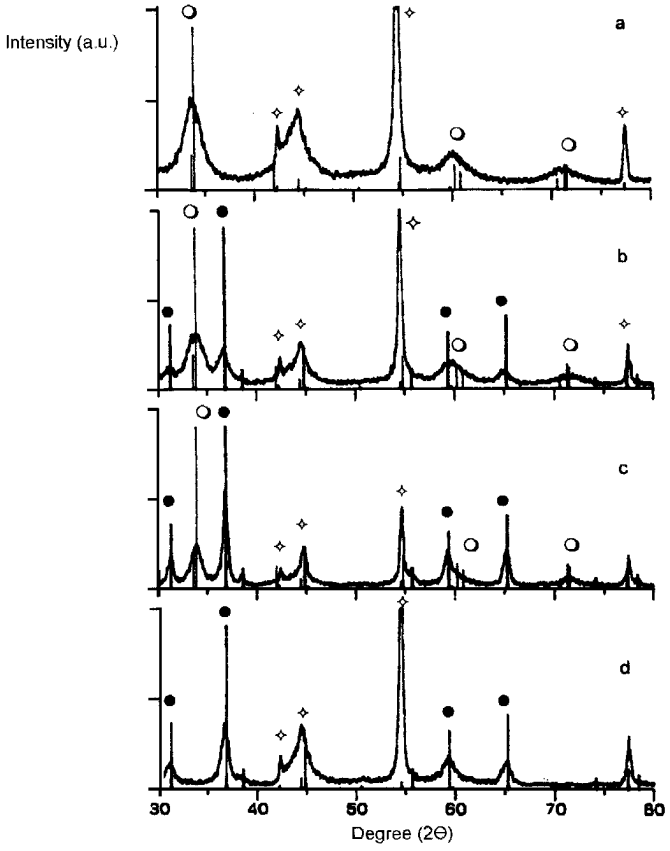

FIG. 1. X-ray diffraction patterns for the calcined catalysts. (a) Pd/G; (b) $Pd_{33}Co_{67}$/G; (c) $Pd_{16}Co_{84}$/G; (d) Co/G. (○) PdO; (●) Co_3O_4; (◇) graphite. Vertical bars indicate position of Bragg peaks for PdO (solid lines) and Co_3O_4 (dashed lines).

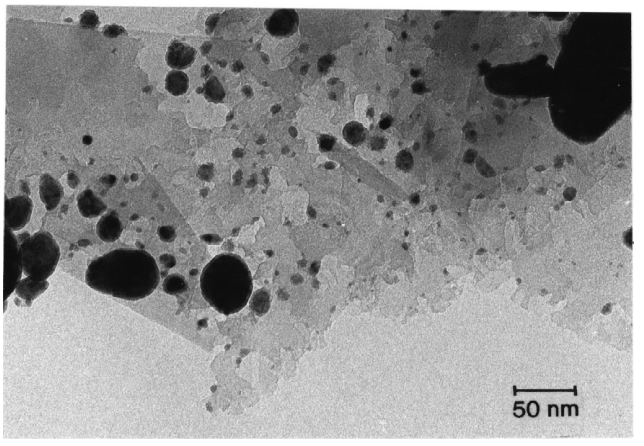

FIG. 2. Transmission micrograph of the $Pd_{16}Co_{84}$/G catalyst after reduction at 773 K and passivation.

Evidence of graphite edge destruction was apparent, indicating that its gasification occurred during the calcination treatment. The destruction of the support appeared more important with cobalt-containing catalysts than with pure Pd/G.

After reduction and passivation, local analyzes by STEM-EDX indicated that the majority of the particles contained both metals. The existence of channels with limited width and important lengths confirmed new localized destruction of graphite (Fig. 2).

TPR1 (TCD Variations)

Figure 3 presents the TPR profiles of the graphite-supported catalysts. The TPR profile of the Pd/G catalyst (Fig. 3a) shows two hydrogen uptakes, one at room temperature and the other at 373 K, and two desorption peaks, at 336 K and between 408 and 575 K, respectively. A third hydrogen consumption peak also appears between 573 and 973 K. Note that the reduction profile of pure graphite showed a hydrogen consumption above 673 K, with a maximum at around 964 K.

For the Co/G catalyst (Fig. 3d), two hydrogen uptakes are observed, at 623 and 762 K. In this case, no hydrogen uptake was detected at room temperature.

In the case of the $Pd_{33}Co_{67}$/G and $Pd_{16}Co_{64}$/G bimetallic catalysts (Figs. 3b and 3c), we observed two main hydrogen uptakes after room temperature consumption, 401 and 592 K for $Pd_{33}Co_{67}$/G, 413 and 610 K for $Pd_{16}Co_{84}$/G.

TPR2 (TCD + Mass Spectroscopy Analysis)

The results of TPR performed in the equipment coupling TCD and mass spectroscopy analysis are presented in Fig. 4, which shows the variation for $m/e = 2$, 15, 28, 29, 30, and 44

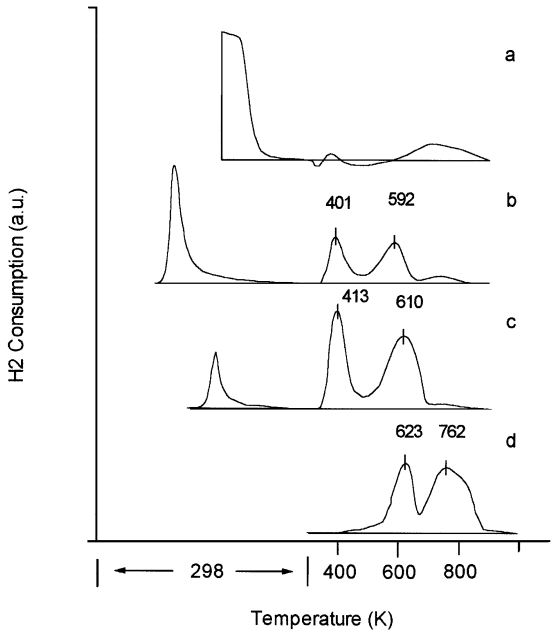

FIG. 3. Reduction profiles of the graphite-supported catalysts obtained by TPR followed by TCD. (a) Pd/G; (b) $Pd_{33}Co_{67}$/G; (c) $Pd_{16}Co_{84}$/G; (d) Co/G.

as opposed to the reduction temperature for each catalyst. For this figure, hydrogen consumption at room temperature was suppressed in order to have a comparable presentation. In the same figure the indicated temperatures were not corrected for the lag time from the reactor to the detector. Therefore, their values are slightly higher than those plotted in Fig. 3.

On the Pd/G catalyst (Fig. 4a), the profile for $m/e = 2$, which corresponds to hydrogen, is very similar to that observed in Fig. 3a. Parallel to hydrogen consumption between 580–1013 K, the trace for $m/e = 15$ (mainly methane) exhibits a maximum at 706 K suggesting that this hydrogen uptake is not due to PdO reduction.

In the case of the Co/G catalyst (Fig. 4b), the situation is more complex. Two hydrogen uptakes are detected, the first with a maximum around 659 K and the second at 786 K, as observed in Fig. 3d. However, in this case, MS analysis shows that the hydrogen uptake around 786 K is associated with the presence of several other compounds. The trace for $m/e = 44$ (mainly carbon dioxide) presents a maximum in the 870–920 K range. The reduction of the same catalyst followed by gas chromatography analysis showed that the $m/e = 28$, 29, and 30 contributions are due to the presence of carbon monoxide, ethane, and ethene. Methane formation ($m/e = 15$) was limited for the Co/G catalyst, showing different behavior of Co and Pd with respect to carbon–hydrogen interaction.

On the bimetallic $Pd_{33}Co_{67}$/G catalyst (Fig. 4c), the formation of methane ($m/e = 15$) and carbon dioxide ($m/e = 44$) was observed. These gases are released at lower temperatures (maximum at 577 and 609 K, respectively) than in the case of both monometallic samples. Compounds corresponding to $m/e = 28$, 29, and 30 species were also observed simultaneously to methane release. On the second bimetallic sample, $Pd_{16}Co_{84}$/G (Fig. 4d), the reduction chemistry appears more simple. Only methane is detected, as an additional species, during the TPR experiment, with a maximum around 760 K.

Table 2 summarizes the hydrogen uptakes measured in the main peaks of the hydrogen reduction profiles. In the case of TPR1, it was not necessary to analyze the variations in conductivity due to hydrogen consumption. In the case of TPR2, the hydrogen uptakes were those calculated from the traces of $m/e = 2$. The agreement between both experimental sets of values is only fair. The differences in the hydrogen uptakes are generally acceptable, except for peak 2, where the differences are important, due probably to the formation of a complex mixture of gases reaching the TCD.

Magnetic Measurements

Figure 5 shows the variations in the magnetization measured at 300 K of $Pd_{33}Co_{67}$/G catalyst as a function of the magnetic field after reduction at 298, 473, and 873 K. Saturation magnetization was determined from the *M(H)* curves and the amount of metallic cobalt expressed as a reduction degree was calculated for each reduced catalyst (35). At 873 K the cobalt species reduced completely to metallic cobalt (Table 3).

TABLE 2

Hydrogen Consumption (μmol H_2/mg Metal) in the Traditional TPR (TPR1) and in the TPR Coupled to Mass Spectrometry Analysis (TPR2)

	TPR1			TPR2			Theoretical[a]		
Catalyst	T_{room}	Peak 1	Peak 2	T_{room}	Peak 1	Peak 2	T_{room}	Peak 1	Peak 2
Pd/g	11.6	−0.7	2.3	12.9	−0.5	4.8	9.4	—	—
$Pd_{33}Co_{67}$/g	7.6	3.0	5.1	6.3	2.6	3.9	4.5	3.0	8.9
$Pd_{16}Co_{84}$/g	2.9	6.2	9.3	2.6	4.6	8.8	2.4	4.2	12.7
Co/g	—	6.0	9.5	—	5.9	11.4	—	5.7	17.0

[a] Theoretical H_2 consumption corresponding to T_{room}, $PdO \rightarrow Pd^0$; peak 1, $Co_3O_4 \rightarrow CoO$; and, peak 2, $CoO \rightarrow Co^0$.

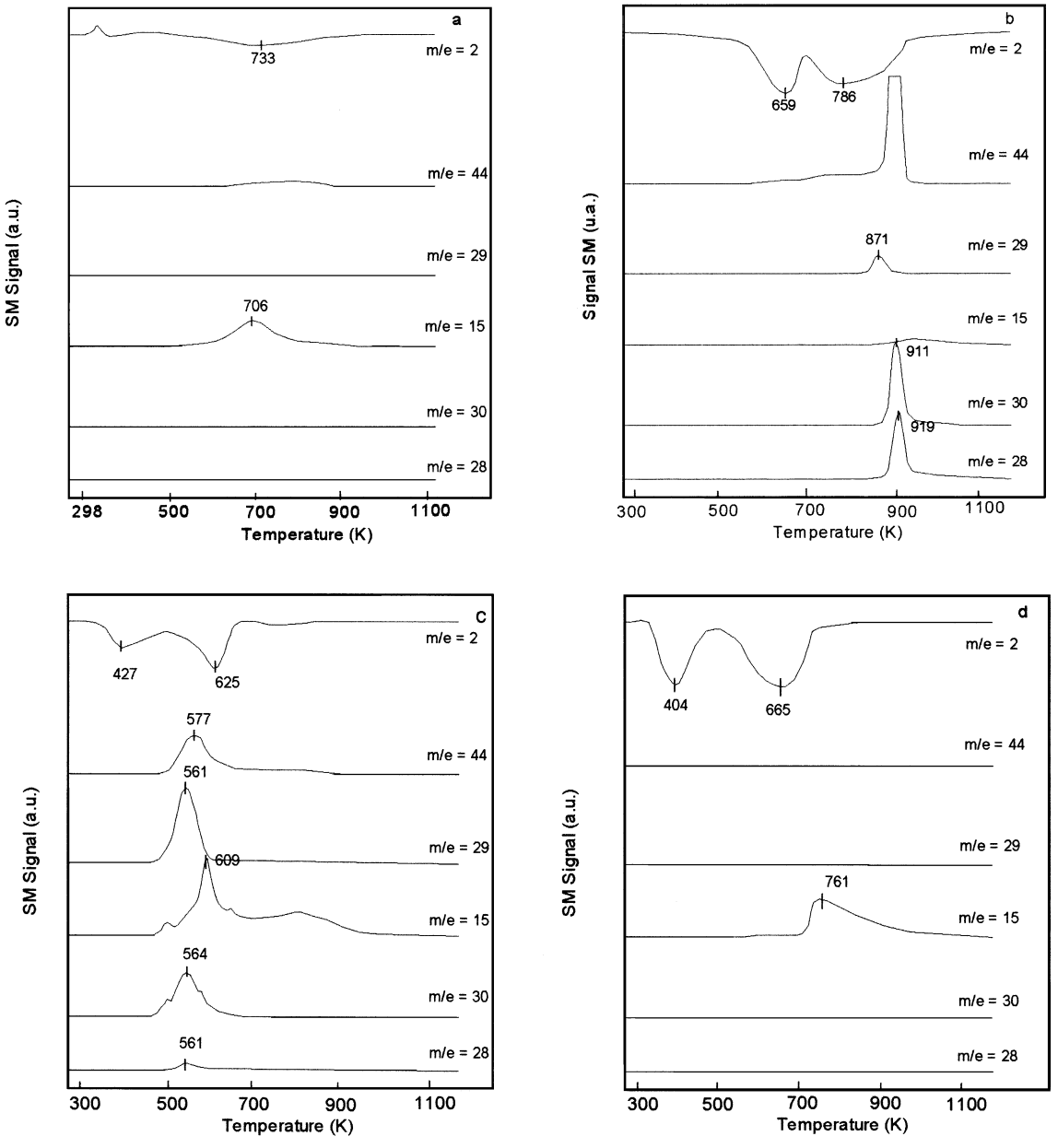

FIG. 4. Variations of $m/e = 2$, 15, 28, 29, 30, and 44 signals as a function of the reduction temperature measured by a TPR coupled to a mass spectrometer for the graphite-supported catalysts; (a) Pd/G; (b) Co/G; (c) $Pd_{33}Co_{67}$/G; (d) $Pd_{16}Co_{84}$/G.

DISCUSSION

State of the Precursors

After calcination at 673 K, X-ray diffraction analysis of all catalysts indicates that both metals are in a completely oxidized state, in the form of PdO and Co_3O_4 (Fig. 1). This means that the calcination treatment, before reduction, did not induce the formation of mixed species, at least not in amounts detectable by XRD. This result is supported by the HRTEM results which allowed the identification of both PdO and Co_3O_4 areas through lattice fringe imaging. Therefore, in the calcined precursors, isolated supported palladium and cobalt oxide particles could be retained as a preliminary model.

However, EDX analyses performed in spot mode showed the presence of palladium and cobalt in a great number of particles, in apparent discrepancy with the idea of fully separated PdO and Co_3O_4 phases. These results led to a model in which a significant fraction of the PdO particles are in physical contact with the surface of the Co_3O_4 particles. Therefore, although PdO and Co_3O_4 appear mainly as seperated crystallographic phases, an interfacial area between PdO and Co_3O_4 may exist, which must be considered

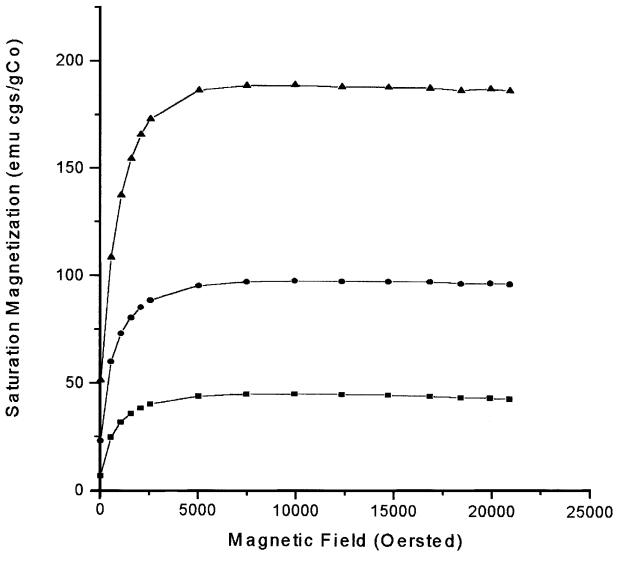

FIG. 5. Magnetization M as a function of magnetic field H for $Pd_{33}Co_{67}/G$, after reduction at 298 (■), 473 (●), and 873 K (◆).

when analyzing the effect of palladium on the reduction of supported cobalt oxide.

Reduction of the Precursor

The TPR equipment generally relies on a thermal conductivity detector (TCD). During temperature-programmed analysis of the graphite-supported catalysts, gasification of the support can occur at high temperature (38), leading to formation of different gaseous compounds such as methane, carbon dioxide, and carbon monoxide (33, 39). Since these gases can be released simultaneously to the hydrogen consumption, the total gas uptake as well as the position of the maxima in the TPR profile might not represent the reductive process itself. However, if conventional TPR equipment is associated with a quadrupolar mass analyzer, not only can a real TPR profile be obtained but other species produced can also be identified, as seen from the results presented in Fig. 4.

TABLE 3

Reduction Degree Calculated from Magnetic Measurements

	Reduction degree (%)		
Catalyst	298 K	Peak 1[a]	Peak 2[b]
Pd/G	—	—	—
$Pd_{33}Co_{67}/G$	25	54	104
$Pd_{16}Co_{84}/G$	0	13	108
Co/G	0	0	100

[a] Peak 1, between 298 and 473 K.
[b] Peak 2, between 473 and 873 K.

On the Pd/G catalyst (Fig. 3a) the hydrogen uptake at room temperature is generally attributed to three different chemical processes: the reduction of palladium oxide, hydrogen absorption in the reduced palladium, and adsorption on the metallic surface (38, 40, 41).

The negative peak at 336 K is due to the desorption of weakly adsorbed hydrogen from the palladium surface and to the decomposition of palladium hydride formed at room temperature. The small peak between 408 and 573 K is attributed to the desorption of strongly adsorbed hydrogen (38, 40, 41). Hydrogen consumption with a maximum around 773 K has been reported in the literature (38), and was ascribed to the reaction of hydrogen with graphite leading to its partial hydrogasification. According to Holstein and Boudart (42), the main product for the carbon–hydrogen reaction catalyzed by platinum is methane. The results from TPR coupled with mass spectroscopy analysis agree very well with this explanation, since methane was detected between 580 and 1013 K.

The reduction profile of the Co/G catalyst shows two hydrogen uptake peaks (Figs. 3d and 4b). After the low temperature peak, the reduction degree was measured by magnetism (Table 3) and did not reveal the presence of metallic cobalt. This is in agreement with the results presented in Table 2, indicating that the hydrogen uptake associated with the low temperature peak is very close to that expected for a complete reduction of Co_3O_4 to CoO. On the other hand, the hydrogen consumption corresponding to the high temperature reduction peak in TPR1 and TPR2 is lower than the value expected for a complete reduction of CoO to Co^0. However, the magnetic measurements revealed that the cobalt oxide was completely reduced after the high temperature peak. In TPR1, the quantification of hydrogen consumption was probably affected by the presence of CO_2, CO, ethane, and ethene in the outcoming gas. In TPR2 results suggested that graphite is playing the role of a reducing agent for the reduction of CoO. This is in agreement with the formation of CO_2 and CO when the reduction temperature reached 870–880 K. Therefore, at high temperature and under a reducing hydrogen atmosphere, a fraction of CoO can be reduced according to the reactions

$$2CoO + C \rightarrow CO_2 + 2Co^0$$

$$CoO + C \rightarrow CO + Co^0.$$

Recently, Gandia and Montes (43) studied the effect of thermal treatments on the properties of cobalt catalysts supported on activated charcoal. The TGA results and XRD patterns showed the reduction of cobalt oxide to metallic cobalt at 723 K under nitrogen atmosphere. According to these authors, the activated charcoal support was able to reduce the cobalt oxide by means of a mechanism in which an important step is the dissolution of carbon atoms in the oxide particles. However, they did not analyze the

outcoming gases during their TGA experiments. In spite of this, their results are in good agreement with the present ones, confirming a possible reduction of cobalt oxide by the carbonaceous support.

On $Pd_{33}Co_{67}$/G catalyst, the presence of 25% of metallic cobalt after reduction at room temperature evidenced a strong promoting effect of palladium on cobalt oxide reduction (Table 3). This result was supported by the hydrogen consumption at room temperature, showing that not only all the palladium oxide, but also a fraction of Co_3O_4 was probably reduced (Table 2). After completion of the hydrogen uptake at 473 K, the magnetism revealed the presence of 54% of metallic cobalt. After reduction at 873 K, a complete reduction of cobalt is deduced from the magnetic data (Table 3), whereas the hydrogen consumption during the TPR was lower than expected for a complete reduction (Table 2). Such a situation, previously observed for the Co/G catalyst, indicates that, besides hydrogen, the graphite support also played a role in the reduction of this catalyst.

In the case of the $Pd_{16}Co_{84}$/G catalyst, the magnetic measurements did not suggest the presence of metallic cobalt after reduction at room temperature (Table 3). Furthermore, the hydrogen uptake deduced from TPR seems to correspond approximately to the reduction of palladium oxide only (Table 2). After reduction at 473 K, the amount of metallic cobalt formed (13%) was lower than that obtained for the $Pd_{33}Co_{67}$/G catalyst. This indicates that a higher cobalt content decreases the promoting effect of palladium, as has been reported for other catalysts (41, 44). However, after reduction at 873 K, a complete reduction of cobalt oxide to metallic cobalt seems to have occurred (Table 3). The results of TPR2 also show hydrogen consumption at high temperature due to the formation of methane induced by the hydrogasification of the graphite.

The gaseous phase associated with graphite gasification is very complex and highly dependent on the catalyst formulation. Results reported in the literature indicate that a direct hydrogasification catalyzed by metals produces mainly methane. CO_2 and CO production is related to the simple solid–solid reaction between graphite and supported CoO. The presence of ethane and ethene could be attributed to secondary reactions between residual hydrogen and water vapor on one hand and to CO, CO_2, and methane on the other.

State of the Reduced Catalysts

As in former studies (10, 44–47), in the present catalysts, the palladium addition shifts the reduction temperature of cobalt species toward lower values. Such a phenomenon is often attributed to an activation of hydrogen followed by hydrogen spillover. However, on the graphite-supported Pd–Co catalysts, it is not necessary to explain the promotion of the reduction of cobalt oxide by a long range hydrogen spillover mechanism only. The electron microscopy results suggested that an important fraction of palladium and cobalt oxide particles are in intimate contact in the precursor state. For the $Pd_{33}Co_{67}$/G catalyst, this contact is probably sufficient to explain, to a great extent, the formation of metallic cobalt at room temperature in the presence of reduced palladium. Such a remarkable promotion is not observed with the bimetallic catalyst which has the lowest palladium/cobalt ratio, i.e., $Pd_{16}Co_{84}$/G. In that case, the room temperature reduction apparently led to reduced palladium only. In both bimetallic catalysts, metallic palladium, existing after reduction at room temperature, must be able to activate hydrogen and promote both hydrogen spillover and metallic cobalt formation. Since no metallic cobalt was formed after reduction at room temperature with the $Pd_{16}Co_{84}$/G catalyst, it is assumed that hydrogen spillover at room temperature does not play an important role during the reduction of this bimetallic catalyst.

Moreover, obtaining bimetallic particles at the end of the reduction is supported by a series of observations:

(i) EDX analysis on reduced and passivated catalysts indicated that the majority of the metallic particles contains both cobalt and palladium, in amounts generally close to the theoretical ones;

(ii) TPR experiments, at the very beginning of the heating ramp did not present clear evidence of a hydrogen desorption peak around 350 K. This peak was observed in the case of the Pd/G catalyst and is due to the decomposition of palladium hydride formed at lower temperature. Its absence is often attributed to alloy formation (47);

(iii) magnetic measurements at the end of the reduction cannot be interpreted as due to pure metallic cobalt alone.

Therefore, an important mobility of the particles, both in oxidized and metallic form, at the surface of the graphite, must be considered during the formation of bimetallic particles and during the reduction steps.

The motion of metallic particles on graphite, a phenomenon eventually associated with catalyzed hydrogasification of the graphite is well established (48–50) and has been studied by various techniques, such as gold-decoration TEM (51), controlled-atmosphere TEM (50), and very recently scanning tunneling microscopy (STM) (52). A hydrogen spillover mechanism was proposed by Rewick *et al.* (53), but seems inconsistent with the zero order reaction, with respect to hydrogen pressure, observed by Holstein and Boudart (42) and Goethel and Yang (50).

In spite of these uncertainties about the mechanism of carbon hydrogasification, particle motion onto the graphite surface was detected; it is important to understand how this phenomenon can influence the formation of bimetallic catalysts.

Thus, we propose that two paths are involved during the reduction of oxidized promoters on the graphite support as

a result of two different Co_3O_4 particles. *At low temperatures*, bimetallic formation is explained by the promoting effect of the metallic palladium on cobalt oxide reduction because both oxides were in intimate contact. *At higher temperatures*, the motion of the metal particles is associated with the gasification mechanisms of the graphite, either hydrogasification when the particles are in a metallic state or oxi/vapogasification when the particles are in an oxidized state. The motions involved in the latter case lead to a higher degree of organisation and of chemical homogeneity of the particles, although their size distribution is very large.

Hence, in the case of Pd–Co bimetallic samples supported on graphite, the migration of particles is probably responsible for the formation of mixed Pd–Co structures at high temperature of reduction.

CONCLUSION

The main conclusions of the present work can be summarized as follows:

—With the present catalysts, and probably with catalysts containing carbonaceous species, a true quantification of hydrogen consumption during TPR cannot be realized with a simple thermal conductivity detector. The use of mass spectrometry is one of the best ways to quantify the hydrogen uptake. When coupled with magnetic measurements, it allowed a better analysis of the various steps involved during the reduction of the cobalt species eventually promoted by the presence of palladium. This promotion took place at temperatures lower than 573 K, probably through a contact between PdO and Co_3O_4 particles and nondestructive migration of cobalt and palladium particles at the surface of graphite;

—At temperatures higher than 673 K, the reduction of residual cobalt is partially performed by a direct interaction between the supported species and the graphite, both for graphite-supported cobalt and for Pd–Co. The motion of the particles due to the graphite gasification could induce new contacts between palladium and cobalt, promoting the reduction of the isolated cobalt oxide particles.

—The gaseous phase produced by the graphite gasification during the activation of the supported catalysts can be a complex mixture, the composition of which depends strongly on the catalysts composition: whereas methane is produced with graphite-supported palladium, ethane, and ethene, together with methane and carbon oxides can be formed when cobalt is present.

ACKNOWLEDGMENTS

F.B.N. is very grateful to CNPq for financial support during his stay in France. The authors thank G. Bergeret and M. T. Gimenez for their contribution to the X-ray measurements.

REFERENCES

1. Reuel, R. C., and Bartholomew, C. H., *J. Catal.* **85**, 78 (1984).
2. Lapidus, A., Krylova, A., Rathousky, J., Zukal, A., and Jancalkova, M., *Appl. Catal.* **A80**, 1 (1992).
3. Castner, D. G., and Santilli, D. S., *in* "Catalytic Materials: Relationship between Structure and Reactivity" (T. E. Whyte, R. A. Dalla Beta, E. G. Derouane, and R. T. K. Baker, Eds.), ACS Symposium Series, Vol. 248, p. 39. American Chem. Soc., Washington, DC, 1984.
4. Silva, R. R. M., Dalmon, J. A., Frety, R., and Schmal, M., *J. Chem. Soc. Faraday Trans.* **89**, 3975 (1993).
5. Takeuchi, K., Matsuzaki, T., Arakawa, H., Hanaoka, T., and Sugi, Y., *Appl. Catal.* **48**, 149 (1989).
6. Xiaoding, X., Doesburg, E. B. M., and Scholten, J. J. F., *Catal. Today* **2**, 125 (1987).
7. Niemantsverdriet, J. W., Louwers, S. P. A., van Grondelle, J., van der Kraan, A. M., Kampers, F. W. H., and Koningsberger, D. C., *in* "Proceedings, 9th International Congress on Catalysis" (M. J. Phillips and M. Ternan, Eds.), Vol. II, p. 674, Chemical Institute, Ottawa, 1988.
8. Zsoldos, Z., Hoffer, T., and Guczi, L., *J. Phys. Chem*. **95**, 798 (1991).
9. Guczi, L., Hoffer, T., Zoldos, Z., Zyad, S., Maire, G., and Garin, F., *J. Phys. Chem*. **95**, 802 (1991).
10. Kapoor, M. P., Lapidus, A. L., and Krylova, A. Y., *in* "Proceedings, 10th International Congress on Catalysis, Budapest, 1992" (L. Guczi, F. Solymosi, and P. Tetenyi, Eds.), part C, p. 2741. Akadémiai Kiadó, Budapest, 1993.
11. Idriss, H., Diagne, C., Hindermann, J. P., Kienemann, A., and Barteau, M. A., *in* "Proceedings, 10th International Congress on Catalysis, Budapest, 1992" (L. Guczi, F. Solymosi, and P. Tetenyi, Eds.), part C, p. 2119. Akadémiai Kiadó, Budapest, 1993.
12. van't Blik, H. F. L., and Prins, R., *J. Catal.* **97**, 188 (1986).
13. Martens, J. H. A., van't Blik, H. F. L., and Prins, R., *J. Catal.* **97**, 200 (1986).
14. van't Blik, H. F. L., Koningsberger, D. C., and Prins, R., *J. Catal.* **97**, 210 (1986).
15. Lee, J., Lee, D., and Ihm, S., *J. Catal.* **113**, 544 (1988).
16. Ho, S., Cruz, J. M., Houalla, M., and Hercules, D., *J. Phys. Chem*. **94**, 6396 (1990).
17. Lee, W. H., and Bartholomew, C. H., *J. Catal.* **120**, 256 (1989).
18. Iglesia, E., Soled, S. L., Fiato, R. A., and Via, G. H., *J. Catal.* **143**, 345 (1993).
19. Summers, J. C., U.S. Patent 255245 881011.
20. Kawai, Y., European Patent 92102540 920214.
21. Ernst, M., Richard, J., and Edward, B., U.S. Patent 734844 910724.
22. Vedage, G. A., Myers, R. S., and Armor, J. N., U.S. Patent 43646 930406.
23. Mallát, T., Szabó, S., and Petró, J., *Acta Chim. Hung.* **124**, 147 (1987).
24. Mallát, T., Szabó, S., Petró, J., Mendioroz, S., and Folgado, M. A., *Appl. Catal.* **53**, 29 (1989).
25. Juszczyk, W., Karpinski, Z., Pielaszek, J., and Paál, Z., *J. Catal.* **143**, 583 (1993).
26. Poutsma, M. L., Elek, L. F., Ibarbia, P. A., Risch, A. P., and Rabo, J. A., *J. Catal.* **52**, 157 (1978).
27. Chin, R. L., and Hercules, D. M., *J. Phys. Chem*. **86**, 360 (1982).
28. Stranick, M. A., Houalla, M., and Hercules, D. M., *J. Catal.* **103**, 151 (1987).
29. Arnoldy, P., and Moulijn, J. A., *J. Catal.* **93**, 38 (1985).
30. Rosynek, M. P., and Polansky, C. A., *Appl. Catal.* **73**, 97 (1991).
31. Sato, K., Ionoue, Y., Kojima, I., Miyazaki, E., and Yasumori, I., *J. Chem. Soc. Faraday Trans. I* **80**, 841 (1984).
32. Zotin, F. M. Z., Tournayan, L., Varloud, J., Perrichon, V., and Fréty, R., *Appl. Catal.* **A98**, 99 (1993).
33. Tomita, A., Sato, N., and Tamai, Y., *Carbon* **12**, 143 (1974).
34. Baker, R. T. K., *Catal. Rev. Sci. Eng.* **19**, 161 (1979).

35. Dalmon, J. A., *in* "Catalysts Characterization" (B. Imelik, and J. C. Védrine, Eds.), p. 791. Plenum, New York, 1994.
36. Dalmon, J. A., *J. Catal.* **60**, 325 (1979).
37. Bozorth, R. M., Wolff, P. A., Davis, D. D., Compton, V. B., and Wemick, J. M., *Phys. Rev.* **B122**, 1157 (1961).
38. Chen, G., Chou, W. T., and Yeh, C. T., *Appl. Catal.* **8**, 389 (1983).
39. Martinez, M. C. R., Amoros, D. C., Solano, A. L., and de Lecea, C. S. M., *Carbon* **31**, 895 (1993).
40. Chang, T. C., Chen, J. J., and Yeh, C. T., *J. Catal.* **96**, 51 (1985).
41. Noronha, F. B., Primet, M., Fréty, R., and Schmal, M., *Appl. Catal.* **78**, 125 (1991).
42. Holstein, W. L., and Boudart, M., *J. Catal.* **72**, 328 (1981).
43. Gandia, L. M., and Montes, M., *J. Catal.* **145**, 276 (1994).
44. Gentry, S. J., Hurst, N. W., and Jones, A., *J. Chem. Soc. Faraday Trans. I* **77**, 603 (1981).
45. Hoff, A., Ph.D., Norges Tekniske Hogskole, 1993.
46. Sarkany, A., Hightower, J. W., and Guczi, L., "13th North American Meeting of the Catalysis Society, Pittsburgh," 1993.
47. Juszczyk, W., Karpinski, Z., Lomot, D., Prelaszek, J., Paál, Z., and Stakheev, A. Y., *J. Catal.* **142**, 617 (1993).
48. Tomita, A., and Tamai, Y., *J. Phys. Chem.* **78**, 2254 (1974).
49. Baker, R. T. K., *in* "Carbon and Coal Gasification" (J. L. Figueiredo, and J. A. Moulijn, Eds.), NATO Series 105, p. 231. Nihoff, Netherlands, 1986.
50. Goethel, P. J., and Yang, R. T., *J. Catal.* **101**, 342 (1986).
51. Henning, G. R., *in* "Chemistry and Physics of Carbon" (P. L. Walker, Ed.), Vol. 2. Dekker, New York, 1966.
52. Chu, X., Schmidt, L. D., Chen, S. G., and Yang, R. T., *J. Catal.* **140**, 543 (1993).
53. Rewick, R. T., Wentrcek, P. R., and Wise, H., *Fuel* **53**, 274 (1974).